International Conference on Space Optics—ICSO 2018

Chania, Greece

9–12 October 2018

Edited by Zoran Sodnik, Nikos Karafolas, and Bruno Cugny

Robust optical design for optimal performance of the MERLIN lidar instrument

Susanne Nikolov

Werner Hupfer

Christian Wührer

Gerald Mathe

et al.

International Conference on Space Optics — ICSO 2018, edited by Zoran Sodnik, Nikos Karafolas, Bruno Cugny, Proc. of SPIE Vol. 11180, 111802A · © 2018 ESA and CNES · CCC code: 0277-786X/18/$18 · doi: 10.1117/12.2536001

Robust optical design for optimal performance of the MERLIN Lidar instrument

Susanne Nikolov[1], Werner Hupfer[1], Christian Wührer[1], Gerald Mathe[1], Alexander Sohmer[1], Stefano Lucarelli[1], Arnaud Chiri[1], Andreas Allgaier[1], Wolfgang Holota[2], Nicolas Paulin[3]
[1]Airbus Defence and Space GmbH, [2]Holota Optics, [3]Safran Reosc

ABSTRACT

The optical design for the **MERLIN instrument** was driven by a concept which ensures reliable, high performance operation of the **bi-static DIAL**, consisting of separate transmitter (TX) and receiver paths (RX). The MERLIN satellite is a secondary passenger payload on the launcher. As such, the satellite places many constraints on the instrument, pertaining to the power, mass and volume allowable. The available resources force the MERLIN instrument to have **passive thermal control** while necessitating a very compact design due to the demanding envelope constraints. This creates a large operational temperature range with thermal gradients on the structure, requiring an extremely robust **optical design** in a **compact envelope**. Typically, a compact envelope requirement drives an optical design towards tight tolerances, which is in contradiction with a large operational temperature range.

The robust optical design, for the RX- and TX-paths, employs several passive measures and an active pointing control for RX and TX co-alignment. These actions are necessary to ensure good instrument performance, despite the demanding environmental requirements. Presented here will be selected load case examples for the entire design and analysis chain, from the instrument performance model towards optical, structural and thermal design.

Keywords: MERLIN instrument, bi-static DIAL, optical design, compact envelope, passive thermal control

1. INTRODUCTION

The joint French-German cooperation Methane Remote Sensing LIDAR Mission (MERLIN) employs an Integrated Path Differential Absorption LIDAR (IPDA) to measure the spatial and temporal gradients of atmospheric CH_4 columns [1], [2]. on a global scale The satellite is being developed and operated by both countries in a joint partnership between the French Space Agency CNES and the German Space Administration DLR. A general overview on the MERLIN mission and a detailed description of the overall instrument architecture is given in [3] and [4] respectively.

The MERLIN LIDAR operates at nadir with a wavelength of approximately 1645nm, where methane has a line sextet offering suitable absorption cross sections and lineshape for implementation of a differential absorption scheme (DIAL). This is implemented by repetitive emission of dual laser pulses at slightly offset laser wavelengths, such that the on-line pulse experiences absorption from the methane feature (referred as λ_{on} at 1645.552 nm) and the other pulse provides a reference for the absorption of the atmospheric column outside the absorption feature (referred as λ_{off} at 1645.846 nm). The absolute methane content can then be inferred from the difference between the "on-line" and "off-line" back scatter signals between instrument and scattering surface. Being an active instrument with its own light source onboard, the MERLIN Lidar instrument does not have to rely on sun illumination and can therefore continuously operate over the orbit at day and night and even through thin cirrus cloud layers [3].

The paper presented here concentrates on the optics layout and the instrument performance connected with it.

2. ENVIRONMENTAL CHALLENGES TO THE MERLIN OPTICS

The MERLIN satellite is supposed to be launched as a secondary passenger together with other satellites. The instrument shall be compatible with the latest generation of the MYRIADE Evolutions Platform. The satellite, with a total mass of 400 kg for platform and instrument together, shall be compatible with the SOYUZ internal position [3]. The payload characteristics are shown in Table 2-1.

Table 2-1: Main instrument characteristics

Parameter	Unit	Payload data
Instrument Mass	kg	150
Instrument Power	W	130
Instrument Volume	mm^3	930 x 850 x 1300
Data Rate	Mbit/s	3.50
Data / Day	Gbit/day	300

The limitations of the envelope enforce a compact instrument design with an elegant arrangement of all subsystems (ref to Figure 2-1). Another important aspect is the orbit selection. For MERLIN, a near-polar sun-synchronous orbit (SSO) with an orbit height of about 500 km, repeat cycle of 28 days and a LTAN of 6am or 6pm is foreseen. In order to increase the compatibility with co-passengers, the satellite design shall be compatible for these two LTAN options [3]. This has a direct impact on the satellite design and increases the operational temperature range for the instrument optics by more than 10°C.

Figure 2-1 Merlin Instrument Iso-View with MLI

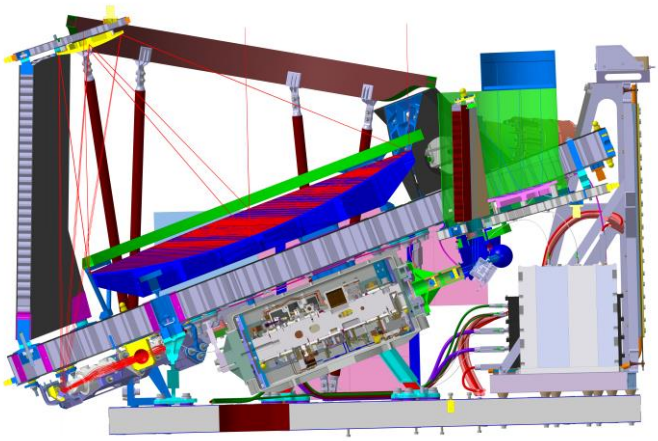

Slice cut through the instrument

Given the limited resources for the instrument, the Thermal Control Subsystem (TCS) relies on passive thermal control elements (MLI, radiators, etc.) integrated by safe heaters during non-operating phases of the instrument.

The implemented main thermal design features are listed below:

- Radiator areas are optimised to the minimum possible sizes, avoiding the need for operational heater power in cold case conditions.
- External surfaces not used as radiators are thermally insulated to the maximum extent possible by means of MLI blankets. Betacloth as an external MLI layer is necessary to fulfil the ATOX requirement.

- The instrument thermal design concept is modular. In general, the instrument is thermally decoupled from the platform, platform to optical bench and intermediate baseplate, hence reducing interface heat fluxes and disturbances. Both, platform and payload, are responsible for their own thermal control, except during non-operational phases.
- Due to the high dissipation of the electrical units and the thermal de-coupling to the platform, its dedicated radiator is oriented towards deep space and is connected to the intermediate baseplate via L-shaped heat pipes.
- Due to the required temperature stability of the laser and detector, both assemblies are decoupled from the optical bench and each assembly has its own radiator. The radiators are located on one of the ±Y sides of the instrument, connected via controlled loop heat pipes.

Except for the laser and the detector, the entire instrument optics and structure has to cope with passive thermal control measures in operational conditions. As a consequence, large temperature ranges and gradients can occur, necessitating the optical design to be tolerant in order to ensure the required instrument performance.

3. PRESENTATION OF THE MERLIN INSTRUMENT OPTICAL DESIGN

3.1 General Description of the MERLIN Instrument Optics Layout

On Figure 3-1 the functional optical block diagram of the MERLIN instrument is shown. From the laser box (LAS), two pulses for the on- and off-line wavelengths are emitted. The pulses pass through the internal calibration chain energy separation unit (ICCS), the active pointing control unit (APC) and finally the transmitter telescope mirrors TXOTP and TXOTS (together TXOT) towards earth. A very small fraction of the outgoing laser pulses is directed to the internal calibration chain and routed towards the Frequency Reference Unit (FRU) and into the receiver chain via 2 integrating spheres and the DEAC (detector assembly calibration optics) onto the detector (SICD).

The receiver telescope consists of the two telescope mirrors RXOTP, RXOTS (together referred as RXOT) and the OCL. The DFL (detector focusing lens) images the incoming signal light backscattered from earth via the RX telescope and the incoming calibration light from the DEAC onto the detector.

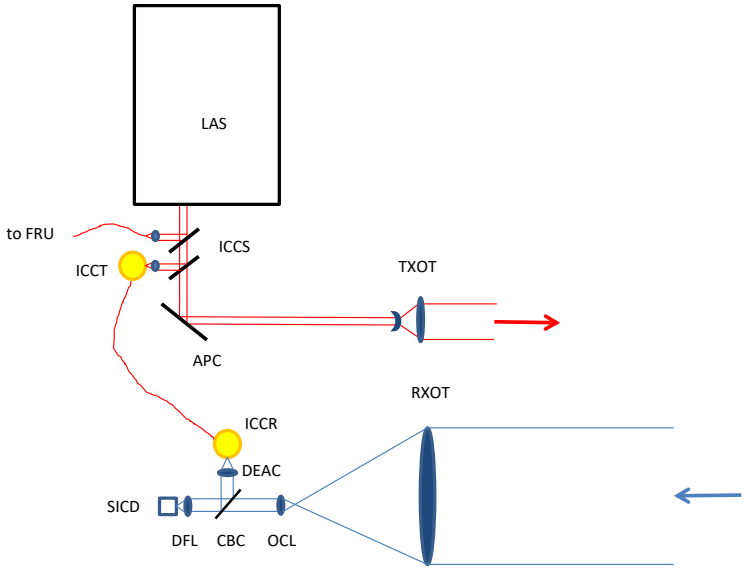

Figure 3-1: Function optical block diagram

The receiver telescope RX is an afocal design with a magnification of 50x. It consists of two conical mirrors and an achromatized ocular lens (OCL), which generates an image of the entrance pupil about 90mm behind the OCL (shown on Figure 3-2). A design driver has been the need for a compact envelope allowing a maximal M1-M2 mirror distance 470mm. This causes the M2 to partly vignette the entrance pupil (3% of the EP area). The DFL focuses the collimated

light from the exit pupil onto the detector. The DFL also contains the narrow-band filter. This filter transmits the narrow window encompassing the two transmission wavelengths and suppresses all remaining detector sensitive light.

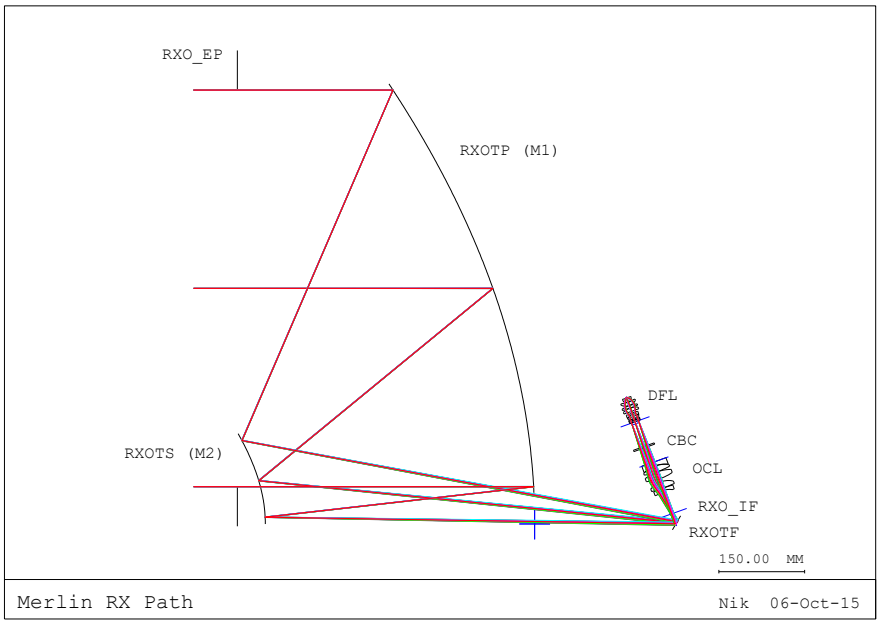

Figure 3-2: Overview of the RX path

The light coming from the M2 passes through a hole in the optical bench and is redirected by the folding mirror RXOTF, parallel to the rear side of the optical bench, but also out of the x-z plane for accommodation reasons. In the intermediate focus (RXO_IF), a field stop is located for protection from out-of-field sun light illumination angles. This field stop is part of the OCL mounting tube.

The RX and TX path principle data are summarized in Table 3-1.

Table 3-1 RX and TX system data

Parameter	Size
RX Entrance Pupil (elliptical)	690mm (off-axis-direction) x 732 mm (on-axis direction)
RX Entrance FOV	1.52 mrad
RX Telescope Magnification	50x
Wavelength	1645 nm (operational) and 633nm (alignment)
RX System Focal Length	470mm
RX System F#	0.64
TX Telescope Magnification	8x
TX Exit Pupil (circular)	150mm

The transmitter telescope consists of the primary TXOTP (M1) and secondary TXOTS (M2) transmitter mirrors, an optical cover window (TXOW), and an active pointing control mirror (APC). The TXOW is required for contamination protection and the APC is necessary for active in orbit co-alignment between the RX and TX beams. The APC mirror is the only active pointing correction element for the optical performance, which ensures an optimal co-alignment between RX and TX footprints on ground. Two wedged glass plates in front of the laser box are used for out-coupling of the reference signals into the laser power and frequency monitoring paths of the internal calibration chain ICC.

The TX Telescope of the MERLIN transmitter path is an afocal telescope with a magnification of 8x. This path belongs to the high energy path, operated with a pulsed 9mJ Laser at λ_{on}=1645.552 nm and λ_{off}=1645.846 nm. The energy density at M2 diameter yields 300mJ/cm2. All elements between the beam exit from the laser box and M2 shall withstand an LIDT value of >10J/cm2 with 48 Hz and <20s pulse length. The entire TX path is encapsulated for contamination protection.

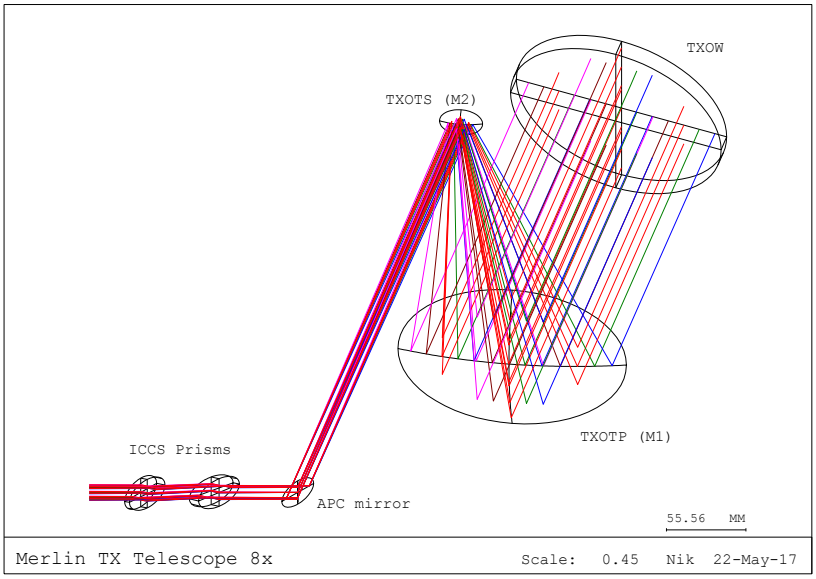

Figure 3-3 Overview of the TX path

For the nominal imaging of the illuminated ground spots, the following design parameter were used in order to cover the three main pointing cases (pointing philosophy). The spot size relations for these pointing cases are shown on Figure 3-4.

- **Initial spot finding** for co-alignment correction between RX and TX path is given by the scan range TX (dotted red circle) within the maximal RX FOV (dotted blue circle) in Figure 3-4. This strong oversizing of the FOV guarantees a high tolerance of the WFE budget against internal variation of the alignment parameters and simplifies the co-alignment of the bi-static system by the possibility to use WFE based alignment methods even if the alignment is not very close to final. A second asset of this oversized FOV is that the operational concept of the APC is based on a scan method allowing clipping on the detector edge. It requires up to a factor 3 FOV oversizing for sufficient signal quality. This mode (by use of the APCM) corrects initial pointing errors of the TX-RX co-alignment caused by ground to orbit effects and the initial on-ground LOS alignment errors for both paths.

- **Performance relevant RX FOV oversizing**
  This mode (by use of the APCM) corrects long term pointing drifts under operational conditions in the instrument. The in-orbit long-term pointing drifts are considered rather small and occur within the 300µm-circle on the image plane (solid line outer blue circle), compared to the initial pointing off-sets for the ground-to-orbit shift.

- **Performance relevant instrument measurement stability**
  This mode ensures the instrument performance without operating the APCM for correction for any short time drifts between the pointing calibration cycles. With the performance model, a maximal pointing error resulting from the structural-thermal and optical analysis has been derived and the results discussed in chapter 4.

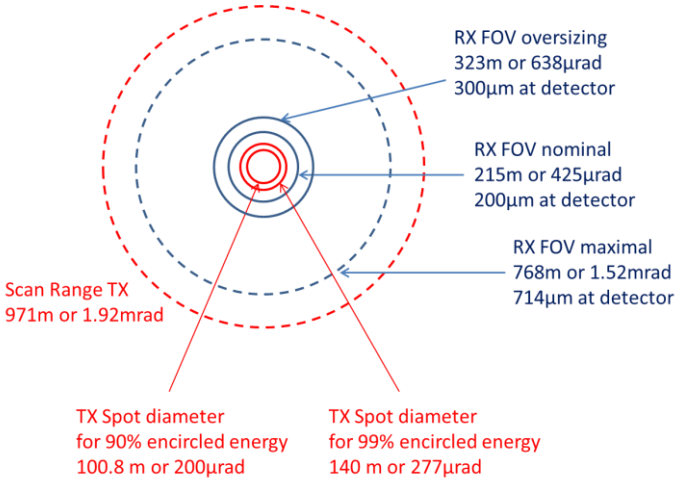

Figure 3-4 Spot size relations on-ground

The optical image quality, including tolerances, remains constant within the three-times oversized the RX FOV and ensures the reliable operation of the MERLIN RX telescope. Also for the TX telescope, the optical performance is ensured within the entire TX Scan range, although the TX telescope is by far the less challenging design, comparing a magnification of 50x for the RX telescope with magnification of 8x from the TX telescope.

Safran Reosc has been selected as our subcontractor for all of the RX and TX telescope optics, including the lens packages OCL, DFL and DEAC. One supplier for all main components allowed us to find the best balanced solution for the RX and TX optics that ensures a good feasibility and an efficient manufacturing for all design aspects. Safran Reosc's critical design review (CDR) has been successfully passed and hardware manufacturing is in progress at the date of this publication. Figure 3-5 shows the photo of the M1 RX after acid etching. The mirror has been light weighted by approximately 90%. Load cases, which are presented in the next chapter for mirror deformations resulting from opto-mechanical analyses, have been performed by the Safran Reosc engineers.

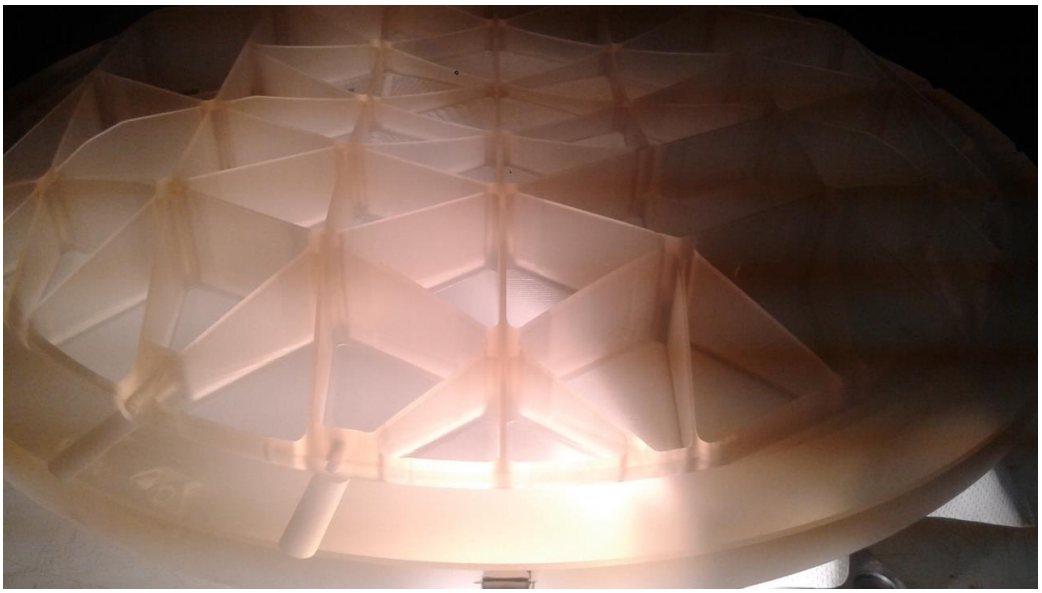

Figure 3-5 Photo of the M1RX QM mirror after acid etching, courtesy of Safran Reosc

3.2 Imaging Performance of the RX path load case examples

The thermal environment for the lowest in-orbit operational temperatures is called the cold case and shows the largest difference with respect to the alignment temperature of 21°C. The hot-case temperatures on the mirrors are approximately 12°C for M1 RX and 7°C for M2 RX. The local temperature distribution on mirror surface for the hot case looks very similar to the cold case shown on Figure 3-6.

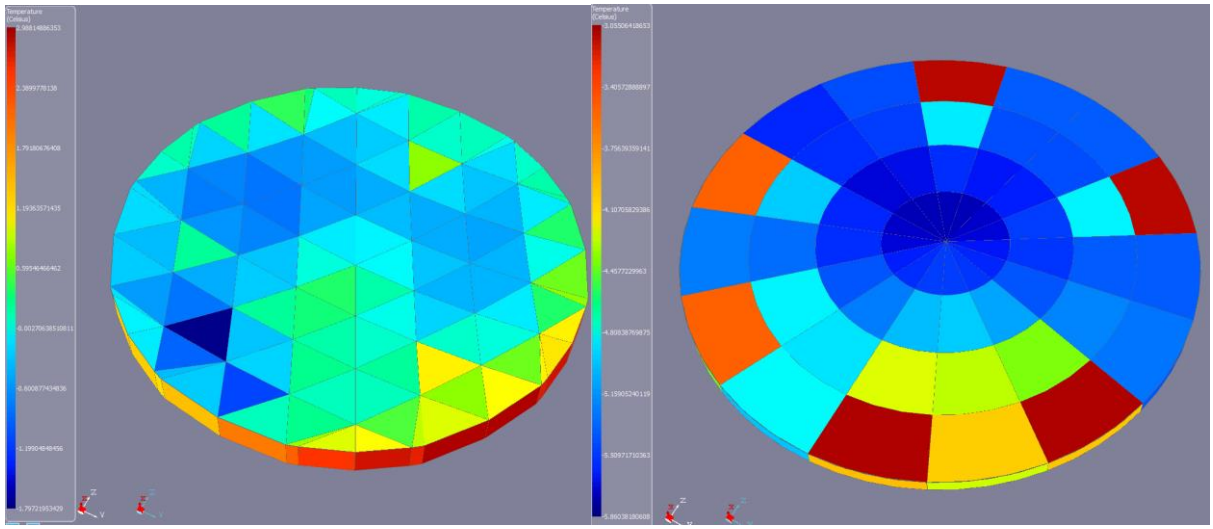

Figure 3-6 M1 RX temperature cold case -5°C M2 RX temperature cold case -10°C

The nominal design WFE of the entire RX path is 0.021 λ rms (34.6nm rms), which is well below the diffraction limit for the operational wavelength and leaves plenty of margin for tolerances. The specification WFE for the in-orbit stability on both mirrors incl. focus is for all load cases together 269 nm rms (focus added, irregular WFE RSS).

The Safran Reosc team has analysed deformations on the mirrors due to gravity, baseplate/mirror CTE mismatch, flexure/mirror CTE mismatch, air-to-vacuum stress in the coating, coating stress from CTE difference to mirror substrate and several stress load cases due to distorted flexures on the interfaces of the mirror. The flexure distortion cases have been scaled with random number generation, because these load cases can occur erratically within a certain range. All temperature load and air-to-vacuum contributors are simply summed up with correct sign. All these surface deformations are superimposed on each mirror and used for the calculation of the RX system WFE (pupil map) and the point spread function (PSF). The calculated PSF from the optical analysis and the pointing from all elements in the entire RX path, i.e. mirrors, lenses and structure are the input parameter for the performance analysis in chapter 4.

As an example the unit load case for the flexure/mirror CTE mismatch corresponding to a variation of the temperature of the assembly equal to 1°C is shown on Figure 3-7. In the optical model all unit load cases are multiplied by the appropriate scaling factor.

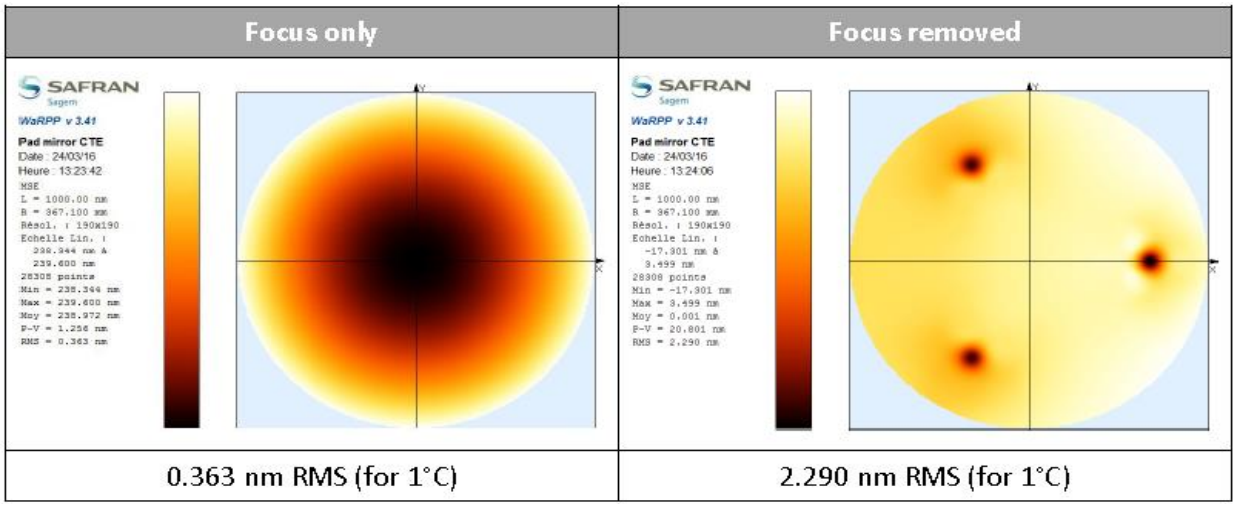

Figure 3-7 Unit load case on M1 RX for the flexure/mirror CTE mismatch

The structure deformation has been analyzed by the Airbus team and includes moisture release of the CFRP due to air-to-vacuum superimposed with the expected thermo-elastic deformations for the largest offset to the alignment temperature. This structure load case is called the nominal case, because it shows typical expected structure deformations from the analysis which is currently still ongoing. Figure 3-8 shows the M1 CFRP baseplate and the M2-tower CFRP structure for the Structure and Thermal Model (STM).

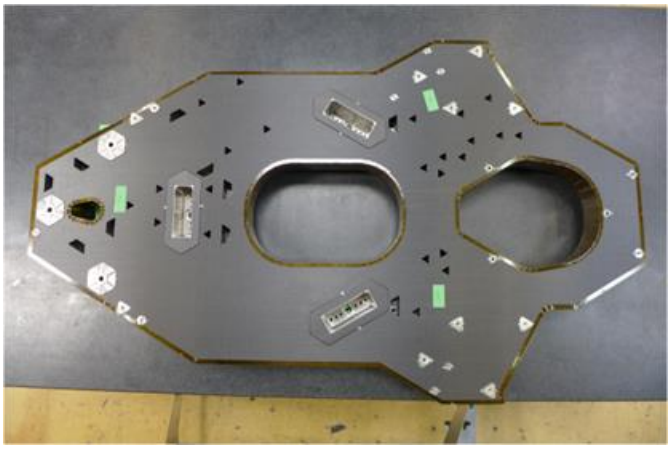

Figure 3-8 STM M1 baseplate

STM M2 tower

The most sensitive tolerances for the nominal structure deformations are:

M1-M2 distance: 12 µm
M2 decenter: 15 µm
Detector defocus: 5 µm

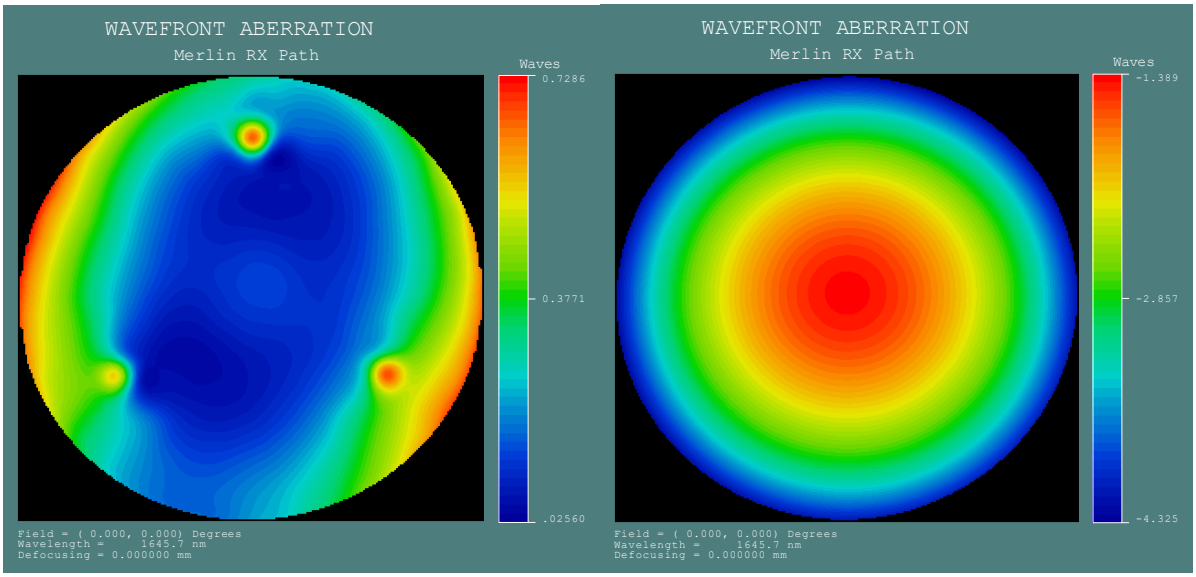

Figure 3-9 RX WFE from mirror load cases M1 and M2 RX WFE from nominal structure deformation
Spot size at detector 7.6 µm rms, 32µm 100% Spot size at detector 18 µm rms, 28µm 100%

The result from the superposition of all mirror interferograms in an ideal structure is 0.164 λ rms (270 nm rms) and the contribution of RX M1 and M2 alone without the RX path design WFE of 34.6 nm rms is 268 nm rms. So the analysis shows that the specification of the in-orbit-stability for the mirrors will be met.

The calculation of the WFE for RX path with the nominal structure deformation and ideal mirrors leads to a WFE of 0.8λ rms (1.3µm rms). The main aberration for the structure deformations is defocus, which will be already partly compensated by the mirror WFE. Taking into account also the influence of the lens packages OCL and DFL whose largest contributor is the refractive index change from air to vacuum it can be shown on the next figure, that for the ground-to-orbit effects no alignment compensation on ground is necessary. The RX path remains focused within the allowed tolerances.

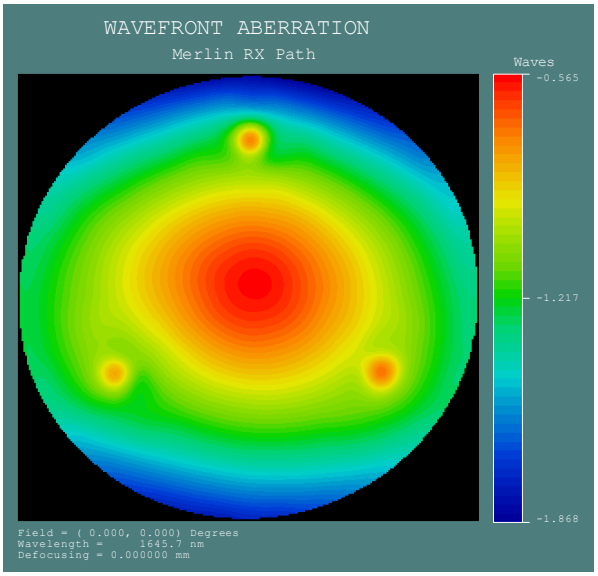

Figure 3-10 nominal RX system WFE 0.28 λ rms (469 nm rms) and spot size 5 µm rms, 30µm 100%
with all contributions from structure, mirrors and lens packages

That means for the nominal optical performance all ground to orbit effects cancel each other out within the tolerances and therefore no pre-compensation for the alignment on-ground is necessary.

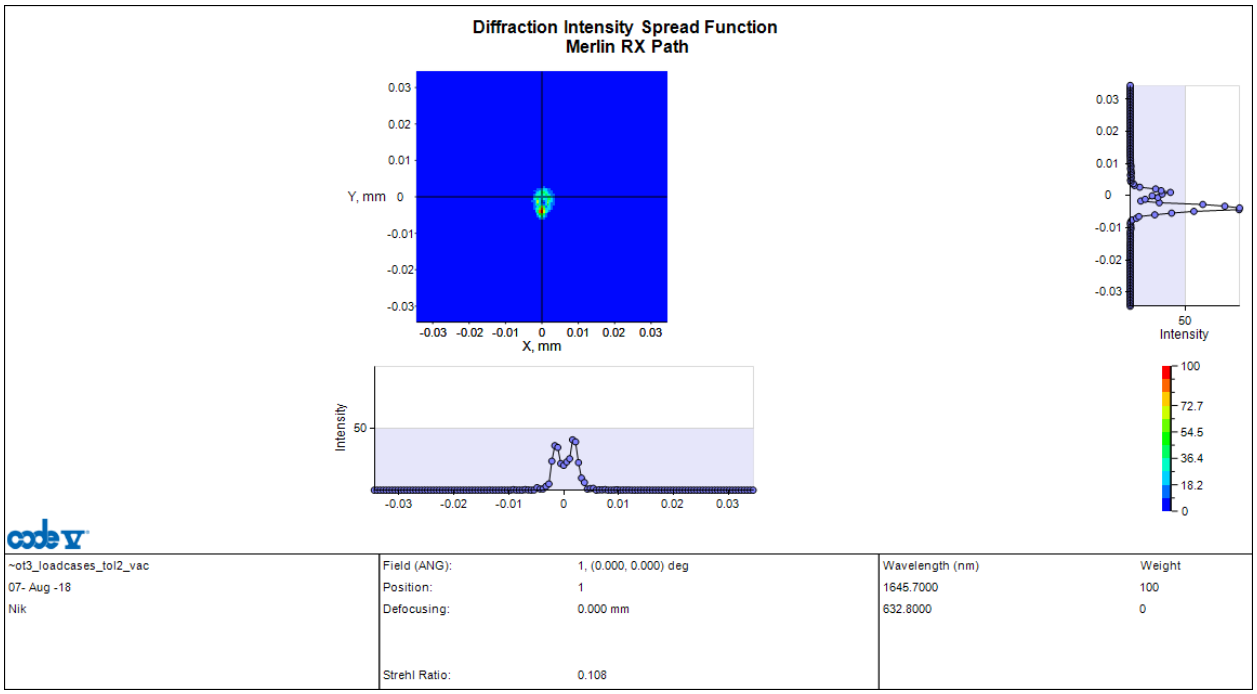

Figure 3-11 PSF of nominal case as input for performance calculation

In order to elaborate the dependency of the MERLIN instrument performance on the RX PSF two other load cases with larger structure deformations than expected have been generated, here referred as high and extreme.

Load Case High		Load Case Extreme	
M1-M2 distance:	15µm	M1-M2 distance:	25µm
M2 decenter:	18 µm	M2 decenter:	20 µm
Detector defocus:	8µm	Detector defocus:	12 µm

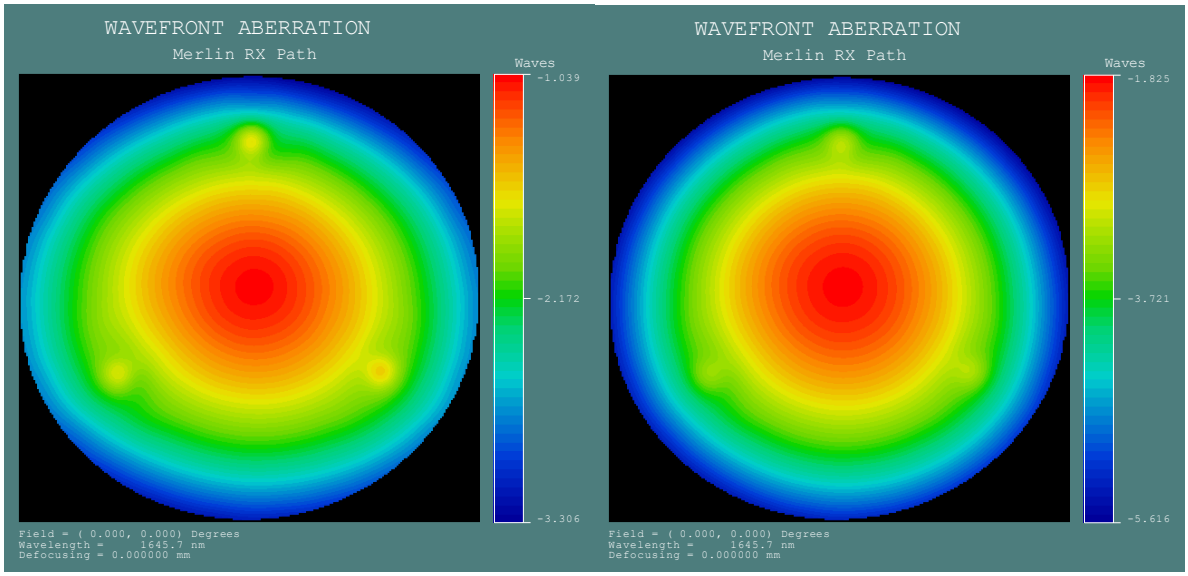

Figure 3-12 Case High: Spot size 10 µm rms, 32µm 100% WFE 0.55 λ rms (905 nm rms)

Case Extreme: Spot size 19 µm rms, 42µm 100% WFE 1.01 λ rms (1.6µm rms)

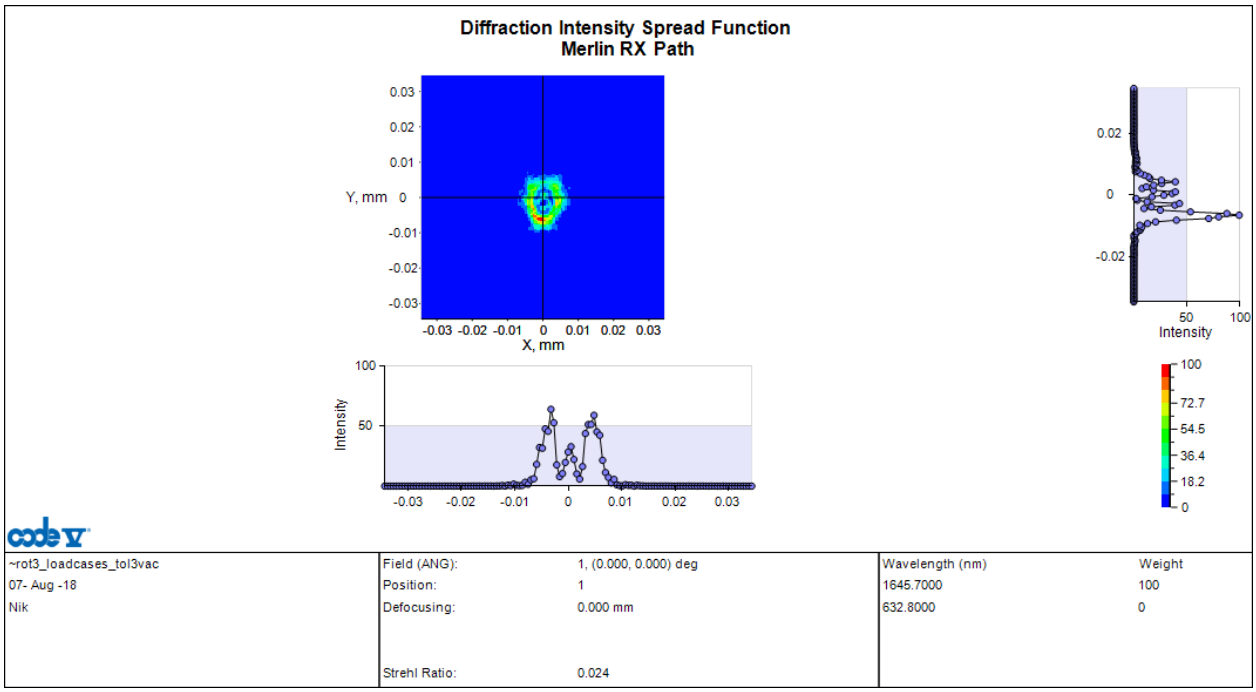

Figure 3-13 PSF for load case high

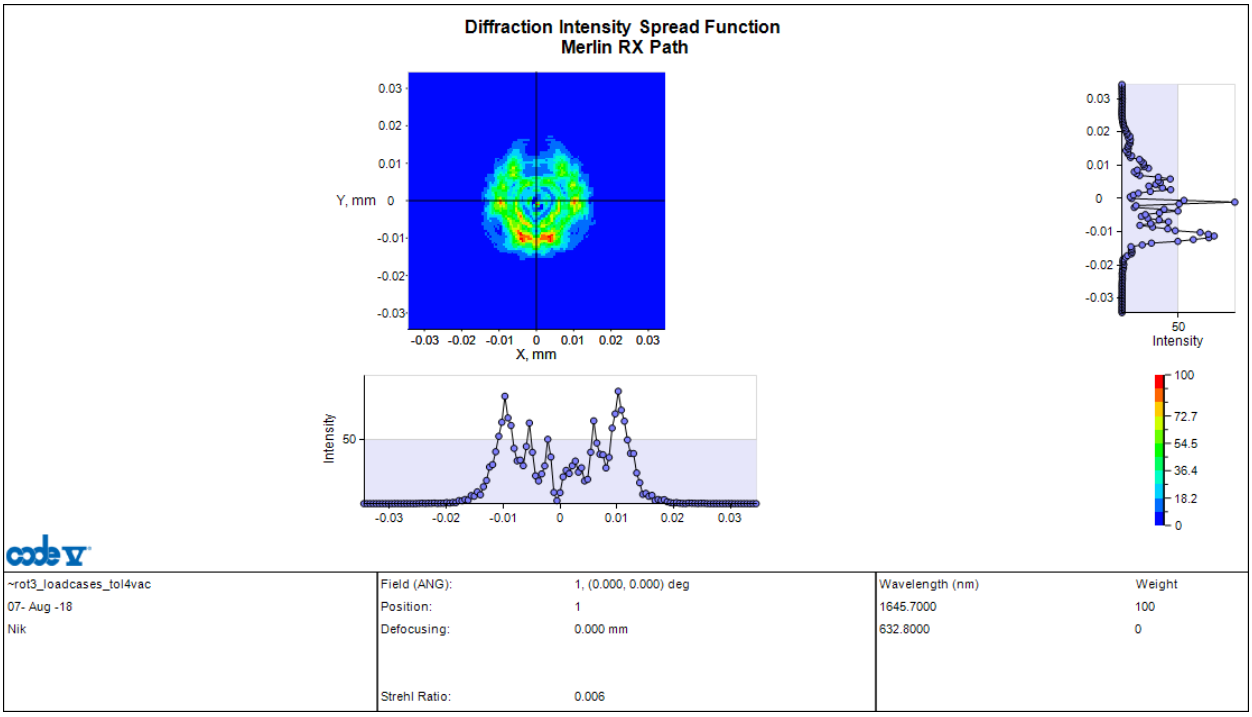

Figure 3-14 PSF load for case extreme

The load cases high and extreme have been generated for parametric analysis of the instrument performance dependency on the RX image quality. The results of this parametrical performance analysis will be discussed in the next chapter.

4. INSTRUMENT PERFORMANCE CALCULATION

The main asset of an active instrument compared to a passive one is the system is essentially self-calibrating. Therefore the critical systematic error of such a system is up to one order of magnitude better for a LIDAR instrument. To maintain the strength of the instrument concept this performance parameter is the most prominent value for the mission. This is reflected in the DAOD Relative Systematic Error (RSE) with a requirement of 0.02% for the contribution of the optical and mechanical instrument design. There are several contributors to the overall RSE budget. One is due to pointing errors from the combination of TX-RX co-alignment and λ_{on}-λ_{off} deviations and stabilities. For the laser specifically these are the systematic line of sight deviation between the λ_{on} and λ_{off} spots and the directional stability of each spot.

The error consists of two parts, which have a difference in energy clipping by the circular APD between the imaged λ_{on} and λ_{off} spots and the optical transmission behavior of all optical elements in the chain for the received pulses and the instrument internal calibration pulses. As the detailed development of some optical components is still ongoing, here only the clipping aspect is considered.

4.1 Pointing Error geometry

The individual pointing error probability spaces are shown schematically (not to scale!) in Figure 4-1 which consist of:

- Probability space of the TX-RX co-alignment (red dashed circle). It is the offset between the APD centre and the centre of the λ_{on}- λ_{off} spot pair. A Gaussian distribution with 0-p (3-sigma) is used.
- Systematic line of sight deviation between the λ_{on} and λ_{off} spot centres (green rectangle), having different values along track and across track, therefore a rectangular shape. Because the exact statistics is currently not known, a worst case is taken in the analysis with 2 extreme corner points.
- Probability space of the directional laser beam stability of λ_{on} and λ_{off} (violet and blue circles). A Gaussian distribution with 0-p (3-sigma) is used.

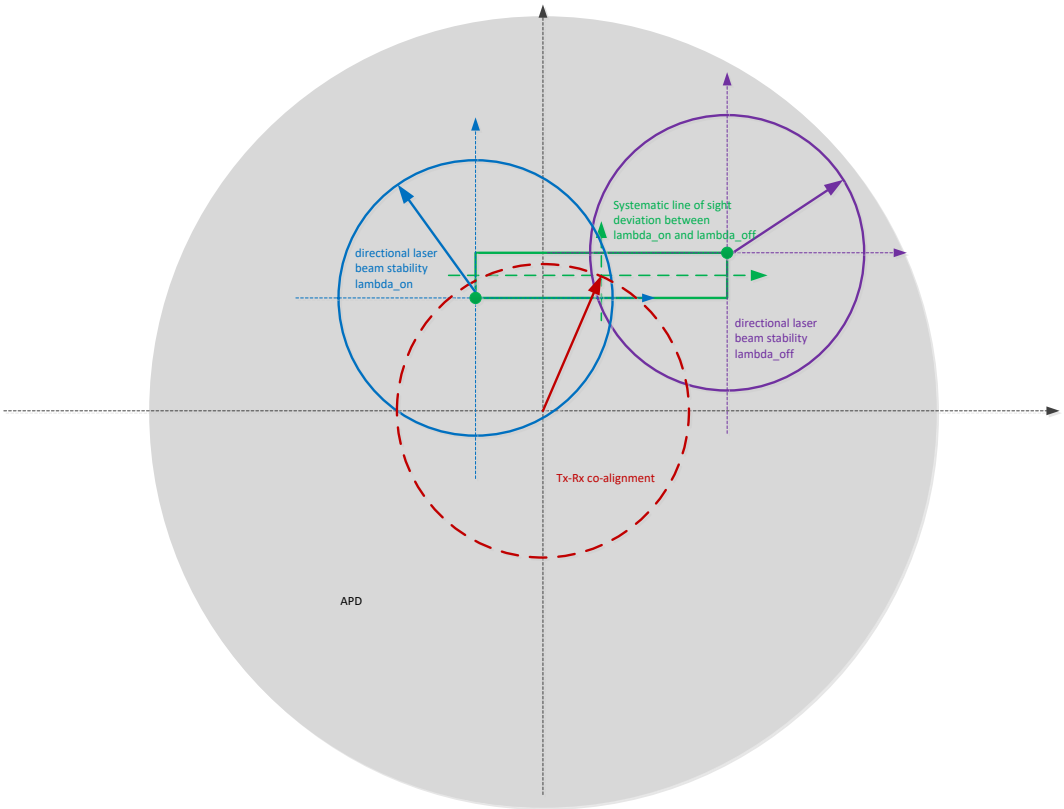

Figure 4-1 Probability space of individual pointing errors

4.2 RSE due to Pointing Errors

The RSE contribution from pointing errors was performed by Monte-Carlo Analysis. The simulation consists of placing the received λ_{on} and λ_{off} laser spots according to the probability space described above in the APD plane. In the analysis three parameters are varied:

- Three PSF load cases from RX, as described above. Both Gaussian laser spots are convolved with the corresponding PSF maps and clipping of the spots by the circular APD is applied
- Ground spot sizes for 90% encircled energy from the TX of 80, 90, 100, 110 m
- The parameter TX-RX co-alignment is varied in the range 0-30m.

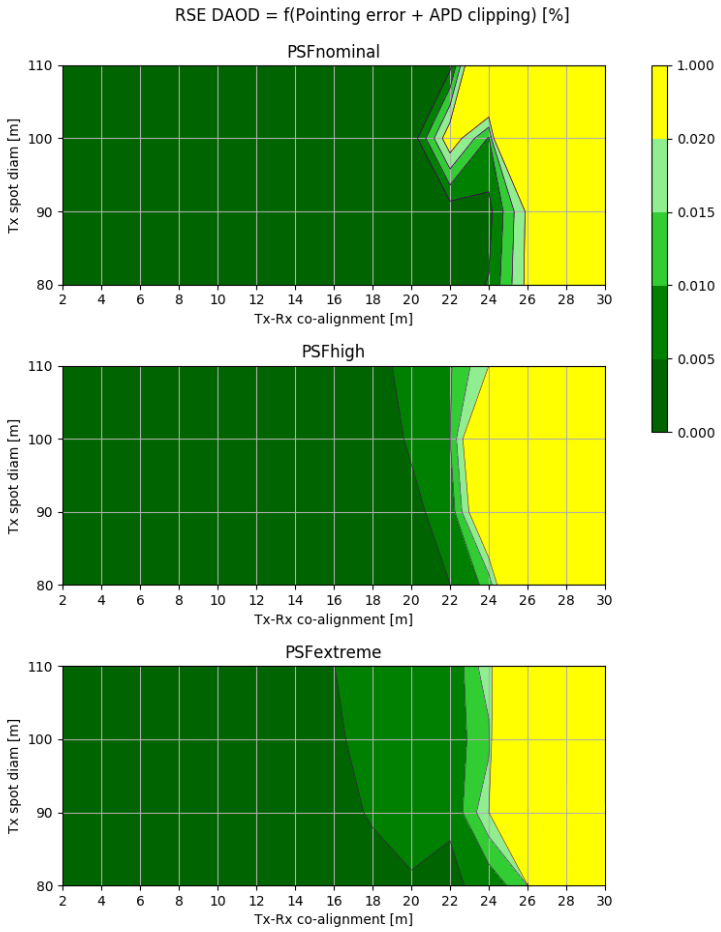

Figure 4-2 RSE as function of PSF load case and TX-RX co-alignment

Figure 4-2 shows the results in form of a contour diagram. The green area is the acceptable range for the pointing error RSE with 0-0.02%. The current allocation for the TX-RX co-alignment error is 15m. The diagram shows, that for 15m the respective RSE contribution is well below the 0.02% limit for all PSF load cases.

The nominal load case, which is the expected mirror and structure performance result of the STOP analysis, would leave 22m for the TX-RX co-alignment mismatch on-ground for all TX spot size variations. The TX spot diameter variation takes into account the expected tolerances for the TX path. The detailed STOP analysis for the TX path is for the time of the publication still in progress.

As mentioned above, the performance analysis was only calculated for the geometrical overlap between RX and TX ground spots and their unsymmetrical clipping by the APD. The large parameter space within the green area of the nominal case can be used for balancing the transmission error contributions with a comfortable margin and ensures still the RSE requirement of 0.02%.

Even for the two hypothetical RX load cases with high and extreme structure deformation some margin within the green parameter space is left for the required RSE of 0.02%.

5. CONCLUSION

The MERLIN instrument design presented here is a robust optical design that enables an active instrument with the laser source onboard to cope with passive thermal control and tight envelope constraints. Such an environment results in a large operational temperature range with thermal gradients on the structure. Therefore the Merlin instrument requires an extremely robust optical design. This has been demonstrated on the presented load case examples for the entire design and analysis chain from instrument performance model towards optical design and structure and thermal design. The results of instrument performance calculation show that the RSE requirement will be met with margin for the optical performance on spot size and pointing.

6. ACKNOWLEDEMENT

The authors would like to thank the whole MERLIN project team at DLR, CNES, Airbus DS, SpaceTech, Fraunhofer ILT, von Hoerner & Sulger, Safran Reosc, and Scisys for their continuous support and their fruitful cooperation in this challenging project. The German part of the MERLIN project is funded by the German Federal Ministry for Economic Affairs and Energy under DLR contract 50 EP 1601.

REFERENCES

[1] C. Stephan et al., “MERLIN - a space-based methane monitor”, Lidar Remote Sensing for Environmental Monitoring XII, *Proc. of SPIE*, Vol. 8159, (2011).
[2] P. Flamant, G. Ehret, B. Millet, M. Alpers, “MERLIN: a French-German mission addressing methane monitoring by LIDAR from space”, *Proc. of 26th ILRC*, Porto Heli, Greece, (2012).
[3] M. Bode, C. Wührer, M. Alpers, B. Millet, G. Ehret, P. Bousquet, "MERLIN: An Integrated Path Differential Absorption (IPDA) Lidar for Global Methane Remote Sensing", Proceedings of ICSO 2016, Biarritz, France 18-21 Oct. 2016.
[4] M. Bode, C. Wührer, C. Kühl, S. Lucarelli, "MERLIN: Overview of the design status of the Lidar Instrument", Accepted Presentation No. 113 at the ICSO 2018, Chania, Greece 09-12 Oct. 2018